

DEVELOPMENTAL BIOLOGY

Hematopoietic stem cells temporally transition to thrombopoietin dependence in the fetal liver

Yejin Lee, Emily DiMaulo-Milk, Juliana Leslie, Lei Ding*

Tissue stem cells temporally change intrinsic mechanisms to meet physiological demands. However, little is known whether and how stem cells rely on distinct extrinsic maintenance mechanisms over time. Here, we found that hematopoietic stem cells (HSCs) temporally transition to depend on thrombopoietin (TPO), a key extrinsic factor, from E16.5 onward in the developing liver. Deletion of *Tpo* reduced mTOR activity, induced differentiation gene expression, and preferentially depleted metabolically active HSCs. Ectopic activation of the JAK2 or MAPK pathway did not rescue HSCs in *Tpo*^{-/-} mice. Enforced activation of the mTOR pathway by conditionally deleting *Tsc1* significantly rescued HSCs and their gene expression in *Tpo*^{-/-} mice. *Lin28b* intrinsically promoted mTOR activation in HSCs, and its expression diminished over time. Conditional deletion of *Lin28b* further reduced mTOR activity and strongly exacerbated HSC depletion in *Tpo*^{-/-} mice. Therefore, HSCs temporally transition from intrinsic LIN28B-dependent to extrinsic TPO-dependent maintenance in the developing liver.

INTRODUCTION

Tissue stem cells change their properties and function throughout life. However, how stem cells transition through these changes over time is still elusive. In the hematopoietic system, hematopoietic stem cells (HSCs) with robust engraftment capacity first appear in the liver at around embryonic day (E) 12.5 in mice (1). These fetal HSCs rapidly self-renew to amplify the stem cell pool. Around birth, HSCs seed the bone marrow, assume the adult identity, and become largely quiescent (1). In addition to cell cycle status and tissue residence, HSCs also undergo changes of surface markers, differentiation potential, transcriptome, and epigenome across ontogeny (2, 3). It has been proposed that the HSC fetal-to-adult identity transition occurs precisely at 3 to 4 weeks postnatally (4). However, recent single-cell data suggest that HSCs begin the transition at the transcriptome level during late embryonic stages in a nonsynchronized manner (3).

The changing properties of HSCs during ontogeny suggest that HSCs engage in distinct regulatory mechanisms over time. A number of genes have been shown to regulate either adult or fetal HSCs in cell-intrinsic manners. *Bmi1* (5), *Gfi1* (6), *Etv6* (7), *Eed* (8), and *Ash1l* (9) are required for adult but not fetal HSCs. In contrast, *Sox17* is required for fetal and neonatal but not adult HSCs (10). RNA binding protein LIN28B is a master regulator controlling fetal HSC properties, and its expression gradually declines over time (11). Enforced *Lin28b* expression in adult HSCs and progenitors confers fetal properties, suggesting that it is an intrinsic master regulator of fetal HSC identity (11, 12). However, it is not clear how *Lin28b* governs fetal HSC identity.

Compared with intrinsic mechanisms, little attention has been paid to temporal changes in HSC extrinsic mechanisms. The perinatal cross-organ liver-to-bone marrow migration indicates that HSCs may markedly change their niche and extrinsic mechanisms in this setting. However, some HSCs start to transition to adult identity at late embryonic stages in the fetal liver (3), raising the

questions of whether and when HSCs temporally rely on distinct extrinsic mechanisms during development without changing their residence. In addition, how HSCs make the temporal transition and rely on different molecular mechanisms without losing their stem cell potential has not been addressed.

By signaling through its cognate receptor, myeloproliferative leukemia virus proto-oncogene (MPL), cytokine thrombopoietin (TPO) is a key extrinsic maintenance factor for adult HSCs through regulating their quiescence (13–15). Here, we report that HSCs transition to TPO dependence at around E16.5 in the fetal liver. Metabolically active HSCs particularly relied on TPO in a specific temporal manner. Janus kinase 2 (JAK2), mitogen-activated protein kinase (MAPK), and mammalian target of rapamycin (mTOR) all have been proposed to be downstream of MPL in cell lines (16). Our systemic genetic epistatic analyses identified mTOR as the major pathway downstream of TPO in HSCs during development in vivo. Extrinsic TPO promoted mTOR activity and HSC maintenance cooperatively with intrinsic LIN28B. As intrinsic *Lin28b* expression diminishes over time, extrinsic *Tpo* expression gradually increases to maintain mTOR activity and HSCs. Thus, HSCs temporally change their extrinsic maintenance mechanisms by transitioning to TPO dependence in the fetal liver. Our work reveals a mechanism by which extrinsic factors can temporally gain control on HSCs by coupling to an existing intrinsic pathway.

RESULTS

HSCs transition to depend on TPO from E16.5 onward

TPO is required by adult bone marrow HSCs (15). We thus tested whether HSCs differentially require TPO for their maintenance across ontogeny by analyzing *Tpo*^{-/-} mice at several time points before the adult stage. Because it has been proposed that HSCs switch from fetal to adult identity postnatally at 3 to 4 weeks old (4), we first tested whether *Tpo* is required for the maintenance of HSCs before this transition. Three-week-old *Tpo*^{-/-} mice had significant reductions in bone marrow cellularity, Lin⁻Sca1⁺cKit⁺ (LSK)-restricted hematopoietic progenitors, and CD150⁺CD48⁻LSK HSCs (fig. S1, A to C), suggesting that HSCs start to rely on TPO from an earlier time point. These mice also had significant reductions in CD41⁺ megakaryocytic cells and platelet counts (fig. S1, D and E).

Copyright © 2022
The Authors, some
rights reserved;
exclusive licensee
American Association
for the Advancement
of Science. No claim to
original U.S. Government
Works. Distributed
under a Creative
Commons Attribution
NonCommercial
License 4.0 (CC BY-NC).

Columbia Stem Cell Initiative, Department of Rehabilitation and Regenerative Medicine and Department of Microbiology and Immunology, Columbia University Irving Medical Center, New York, NY 10032, USA.

*Corresponding author. Email: ld2567@cumc.columbia.edu

To pinpoint the exact time at which HSCs transition to *Tpo* dependence, we analyzed mice at several earlier pre- and postnatal stages. At E14.5, *Tpo*^{-/-} mice had normal cellularity, HSC, Flt3⁻ LSK hematopoietic progenitor, LSK, and CD41⁺ megakaryocytic cell frequencies (Fig. 1, A to D, and fig. S1F). E13.5 *Tpo*^{-/-} mice also had normal cellularity, LSK, and HSC frequencies (fig. S1, G to I). Liver cells from E14.5 mice gave normal long-term multilineage reconstitution when transplanted into lethally irradiated recipient mice with normal levels of donor-derived HSCs (Fig. 1, E and F), suggesting that E14.5 HSCs do not rely on TPO. At E16.5, 2 days later, *Tpo*^{-/-} mice had normal liver cellularity (Fig. 1G). However, these mice had a significant reduction in HSC frequency, with normal Flt3⁻ LSK or LSK hematopoietic progenitor frequencies and a modest reduction in CD41⁺ cells (Fig. 1, H to J, and fig. S1J). At postnatal day (P) 0, livers from *Tpo*^{-/-} mice had a nearly 10-fold reduction in HSC frequency with normal cellularity compared with littermate *Tpo*^{+/+} controls (Fig. 1, K and L, and fig. S1K). Notably, *Tpo*^{+/-} heterozygous mice had an intermediate HSC frequency reduction phenotype, suggesting haploinsufficiency. Flt3⁻ LSK, LSK, CD41⁺ megakaryocytic lineage cells, and platelet counts were also significantly reduced (Fig. 1, M and N, and fig. S1, L and M), while other blood cell counts were relatively normal (fig. S1, N and O). Liver cells from P0 *Tpo*^{-/-} mice formed significantly fewer colonies in methylcellulose and had a significant decrease in their capacity of reconstituting lethally irradiated recipient mice (Fig. 1, O and P, and fig. S1P). Limit dilution assay revealed a notable 14-fold reduction in functional HSCs in P0 *Tpo*^{-/-} livers compared with *Tpo*^{+/+} littermate controls (Fig. 1Q). The reduction in liver HSCs could be due to enhanced egress, as HSCs actively seed the spleen and bone marrow at the perinatal stage. To address this, we also analyzed mice at P5, when HSCs are in migration from the liver to the bone marrow (17). HSC frequency was significantly reduced to a similar extent in P5 *Tpo*^{-/-} livers, bone marrow, and spleens (fig. S1, Q to V). Thus, the reduction in HSCs in *Tpo*^{-/-} mice was not due to enhanced migration out of the liver. Together, our data suggest that HSCs temporally transition to depend on TPO from E16.5 during fetal development.

***Tpo* is primarily expressed by hepatocytes, and its expression increases over time**

To identify the source of TPO, we treated *Tpo*^{creER/+}; *Rosa26*^{LSL-ZsGreen} mice (15) with tamoxifen at E13.5 and E15.5 and performed fluorescence microscopy analysis at E17.5. The liver was the major source of TPO, with little if any expression by the kidney or spleen (fig. S2, A and B). Within the liver, hepatocytes were the major producer of TPO (fig. S2, C to U). Consistently, deletion of *Tpo* from fetal hepatocytes using *Alb-cre* or *Afp-cre* led to a significant reduction in HSC frequency in P0 livers (fig. S2, V and W). Thus, hepatocytes are the major source of TPO during development. Consistent with the gradual dependence of HSCs on *Tpo* (Fig. 1, A to Q), its expression level gradually increased over time in the liver (Fig. 1R).

***Tpo* deletion leads to gene expression changes associated with HSC differentiation**

We investigated the mechanisms by which TPO maintains perinatal HSCs. TPO sustains adult HSC quiescence by regulating the expression of key cell cycle inhibitors, *p19* and *p57* (13, 14). Thus, we assessed whether TPO regulates cell cycle of P0 HSCs. Compared with adult counterparts, P0 HSCs cycle significantly more (fig. S3A),

but P0 HSCs from *Tpo*^{-/-} mice had normal cell cycle status with normal expression of *p19* and *p57*, compared with littermate controls. P0 HSCs from *Tpo*^{-/-} mice also had normal annexin V staining (Fig. 2D), suggesting that HSCs were not depleted because of excessive cell death. It has been reported that TPO regulates adult HSC DNA damage response (18). However, we did not observe a significant alteration of γ H2AX levels in P0 HSCs from *Tpo*^{-/-} mice compared with littermate controls (fig. S3B).

To investigate further the mechanisms of HSC depletion, we performed RNA sequencing (RNA-seq) analysis on sorted HSCs. Compared with controls, P0 HSCs from *Tpo*^{-/-} mice had a significant down-regulation of HSC gene signature (e.g., *Esam*, *Procr*, *Mecom*, and *Egr1*) and a concurrent up-regulation of hematopoietic progenitor gene signature (e.g., *Mpo*, *Itgal*, and *Cd48*) (Fig. 2, E and F, and fig. S3C). Consistent with the observed normal cell cycle, cell death status, and γ H2AX levels (Fig. 2, A to D, and fig. S3B), HSCs from *Tpo*^{-/-} mice had similar expression of proliferation, apoptosis, and DNA damage response gene sets compared with controls (fig. S3, D to F). Our data collectively suggest that HSCs are most likely depleted because of differentiation in P0 *Tpo*^{-/-} mice.

***Tpo* deletion preferentially depletes metabolically active HSCs**

We observed a notable depletion of a subset of cells with larger size [higher forward scatter (FSC) in flow cytometry analyses] within the HSC pool from P0 but not E14.5 *Tpo*^{-/-} mice (Fig. 2, G and H). To further characterize these large HSCs, we performed RNA-seq analyses. Compared with HSCs of smaller sizes, large HSCs had 1154 up-regulated and 1471 down-regulated genes (fig. S3G). Genes associated with a metabolically active state, such as *Pdk4*, *Mrpl42*, and *Eif3m*, were among the up-regulated ones (fig. S3G). Gene set enrichment analysis (GSEA) revealed that large HSCs represented metabolically active HSCs with a significant enrichment of expressed gene sets associated with ribosome biogenesis, translation, oxidative phosphorylation, energy production, and mTOR pathway activation (Fig. 2, I and J, and fig. S3, H and I). Since the mTOR pathway is the major cell size and metabolism regulator (19), we directly assessed the activity of this pathway by probing its downstream targets, pS6 and p4EBP1. The levels of both of them were significantly down-regulated in P0 but not in E14.5 LSKs from *Tpo*^{-/-} mice (Fig. 2, K and L), suggesting that TPO promotes the mTOR pathway activation. In addition, we found that *Tpo* deletion led to a significant reduction in overall protein translation in P0 but not in E14.5 HSCs (Fig. 2, M and N). We also evaluated mitochondria mass and activity. P0 HSCs from *Tpo*^{-/-} mice had normal mitochondria mass but reduced activity (fig. S3, J to L). Thus, TPO maintains perinatal HSCs by regulating the mTOR pathway and metabolic activation.

Ectopic activation of the JAK2 pathway does not rescue HSCs in P0 *Tpo*^{-/-} mice

We reasoned that revealing the mechanisms mediating the signaling in HSCs is the key to understand the temporal changes of TPO dependence. After binding to its receptor MPL, TPO can activate multiple pathways (JAK2, MAPK, and mTOR) (16). We systematically assessed the contribution of these candidate downstream pathways in mediating the TPO pathway in HSCs in vivo.

Constitutively active mutations in *Jak2*, *Mpl*, or overexpression of *Tpo* all lead to myeloproliferative neoplasms (20, 21), suggesting

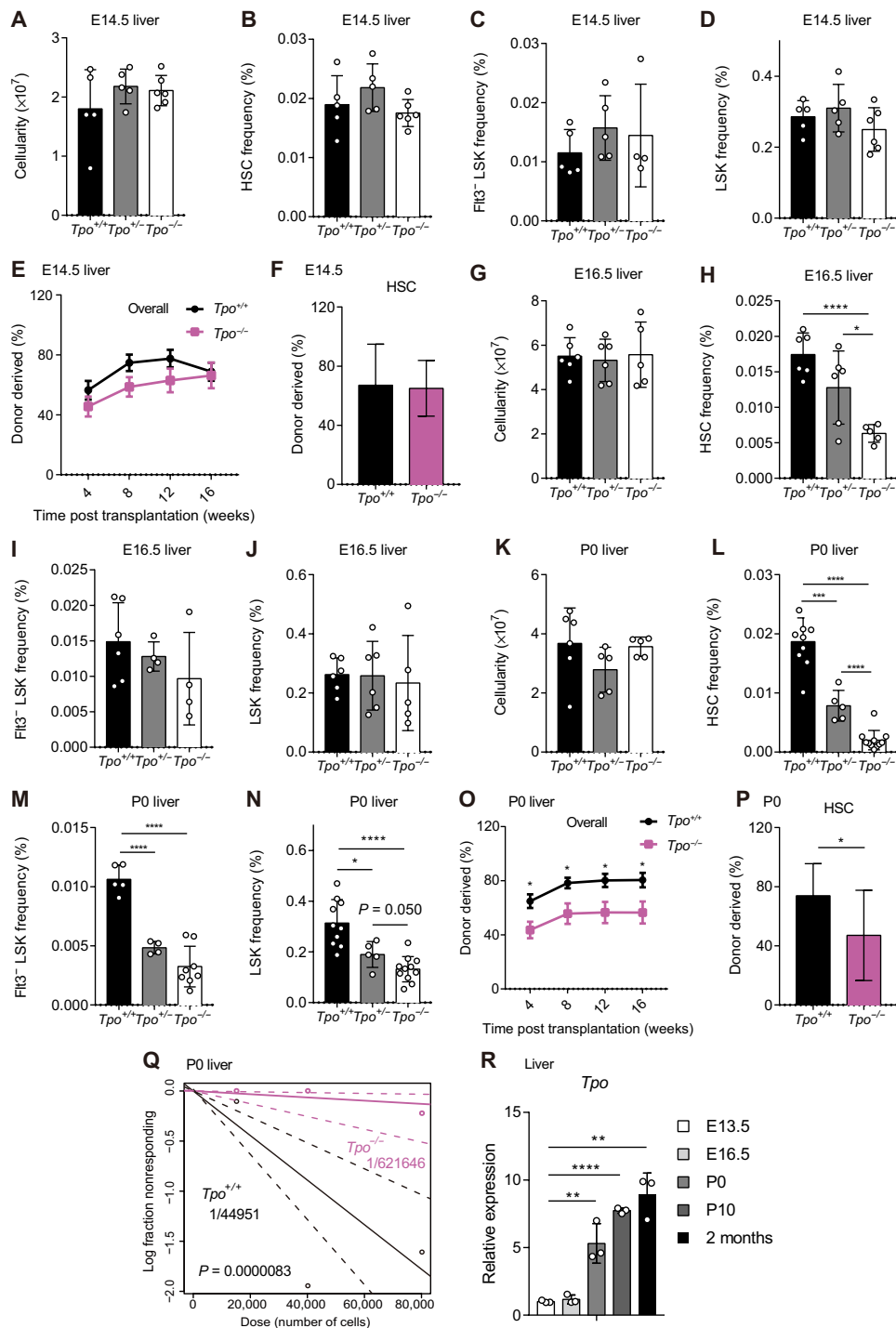


Fig. 1. *Tpo* is not required for HSCs at E14.5 but is required from E16.5 onward. (A to D) Cellularity (A), CD150⁺CD48⁻LSK HSC frequency (B), Flt3⁻LSK cell frequency (C), and LSK cell frequency (D) in E14.5 livers from *Tpo*^{-/-} embryos compared with littermate controls ($n = 4$ to 6). (E) E14.5 liver cells (5×10^5) from *Tpo*^{-/-} embryos gave normal reconstitution in irradiated recipient mice (three independent experiments with a total of $n = 8$ to 12 recipients for each condition). (F) Donor-derived HSC frequencies in recipient mice of (E) 16 weeks after transplantation ($n = 4$ for each condition). (G to N) Cellularity (G), HSC frequency (H), Flt3⁻LSK cell frequency (I), and LSK cell frequency (J) in E16.5 and P0 livers, respectively ($n = 4$ to 11 for each condition). (O) A total of 5×10^5 P0 liver cells from *Tpo*^{-/-} mice gave significantly lower levels of reconstitution in irradiated recipient mice (three independent experiments with a total of $n = 12$ to 14 recipients for each condition). (P) Donor-derived HSC frequencies in recipient mice of (O) 16 weeks after transplantation ($n = 12$ for each condition). (Q) Limit dilution assays show a 14-fold reduction in long-term multilineage reconstituting cells in the P0 liver from *Tpo*^{-/-} mice compared with controls (data represent two independent experiments). (R) *Tpo* transcript levels in the liver at different time points revealed by quantitative reverse transcription polymerase chain reaction (qRT-PCR) analyses ($n = 3$ for each condition). +, wild-type allele; -, germline-deleted allele. All data represent means \pm SD, except in (E) and (O), where data represent means \pm SEM. Two-tailed Student's *t* tests were used to evaluate statistical significance. * $P < 0.05$; ** $P < 0.01$; *** $P < 0.001$; **** $P < 0.0001$.

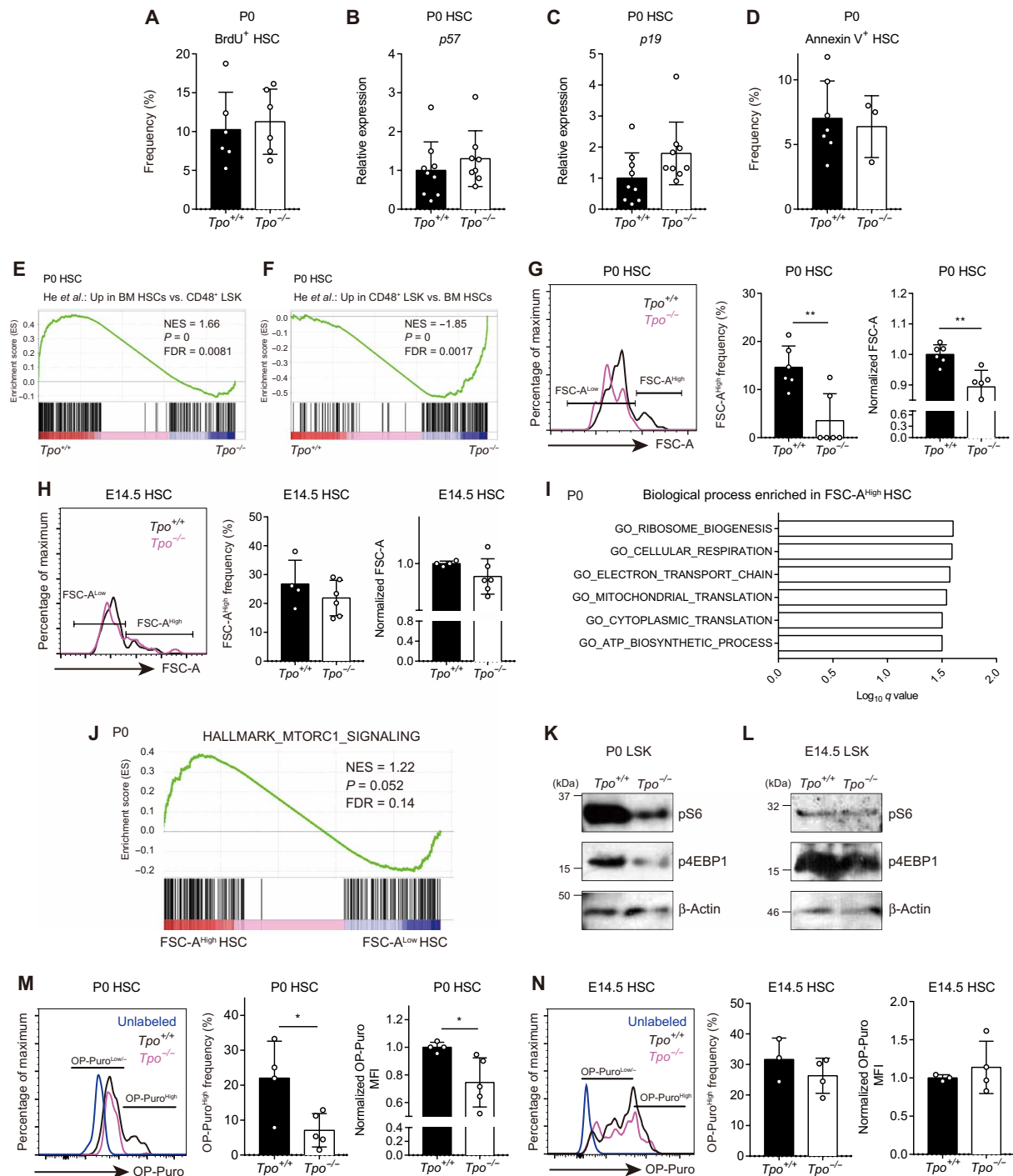


Fig. 2. Deletion of *Tpo* preferentially depletes metabolically active HSCs. (A) Frequency of BrdU incorporated HSCs in P0 livers from *Tpo*^{-/-} mice and littermate controls (*n* = 6 mice for each condition). (B and C) Levels of *p57* and *p19* in HSCs from the livers of P0 *Tpo*^{-/-} mice compared with littermate controls (*n* = 8 to 9 mice for each condition). (D) Annexin V⁺ P0 liver HSC frequency in *Tpo*^{-/-} mice (*n* = 3 to 7 mice for each condition). (E and F) GSEA plots showing that P0 *Tpo*^{-/-} HSCs lose HSC signature genes (E) and gain downstream progenitor signature genes (F) compared with control HSCs (*n* = 4 to 5 for each condition). The signature gene sets were obtained from (46). NES, normalized enrichment score; FDR, false discovery rate. (G and H) Frequency of FSC-A^{high} and normalized FSC-A of HSCs in P0 livers (G) or E14.5 livers (H). Histograms show representative fluorescence-activated cell sorting (FACS) plots (*n* = 4 to 6 mice for each condition). (I and J) Gene ontology analysis and GSEA showing biological processes and mTORC1 signaling genes enriched in FSC-A^{high} compared with FSC-A^{low} HSCs from P0 livers, respectively. (K and L) Western blot of pS6, p4EBP1, and β-Actin in freshly purified LSK cells (lysates from 20,000 to 30,000 cells per lane) from P0 (K) or E14.5 livers (L). (M and N) Frequency of OP-Puro^{high} and normalized OP-Puro fluorescence intensity of HSCs in P0 (M) or E14.5 livers (N). Histograms show representative FACS plots. The fluorescence intensity of OP-Puro in *Tpo*^{+/+} HSCs was used for normalization (*n* = 3 to 5 mice for each condition). OP-Puro (O-propargyl-puromycin). +, wild-type allele; -, germline-deleted allele. Data represent means ± SD. Two-tailed Student's *t* tests were used to evaluate statistical significance. **P* < 0.05; ***P* < 0.01.

that the JAK2 pathway acts downstream of MPL and TPO at least under adult pathological conditions. We ectopically activated JAK2 by recombining a conditional *Jak2*^{V617F} allele (*Jak2*^{CA}) (22) in the germ line (*Jak2*^{VF}). Adult, but not P0, *Jak2*^{VF/+} mice had increased HSC frequency and number (fig. S4, A to J). It was possible that one allele of *Jak2*^{VF} did not sufficiently activate the pathway in P0 HSCs. Thus, we looked for ways to further increase the activity of JAK2 by generating mice with two *Jak2*^{VF} alleles. Because homozygous *Jak2*^{VF/VF} mice are embryonic lethal (22), we increased the dose of *Jak2*^{V617F} by conditionally recombining the other *Jak2* allele through generating *Jak2*^{VF/Δ} mice using *Vav1-cre* (23) specifically in the hematopoietic system (Δ indicates *Jak2*^{V617F} expression specifically in the hematopoietic system induced by *Vav1-cre*). The *Jak2*^{CA} allele was efficiently recombined, leading to significant up-regulation of phospho-signal transducer and activator of transcription 5 (STAT5) in P0 HSCs from these mice (fig. S4, F and G). P0 *Jak2*^{VF/Δ} mice had normal liver cellularity, HSC frequency, number, and CD150⁺CD48⁺ LSK multipotent progenitor (MPP) and LSK frequencies (fig. S4, H to L), indicating that ectopic JAK2 activation does not significantly affect perinatal HSCs.

To test whether the JAK2 pathway mediates TPO signaling in HSCs during development, we generated *Tpo*^{-/-}; *Jak2*^{VF/+}, or *Tpo*^{-/-}; *Vav1-cre*; *Jak2*^{VF/Δ} mice. Relative to littermate *Tpo*^{-/-} mice, P0 mice with ectopic activation of JAK2 had comparable liver cellularity, HSC frequency, number, and CD150⁺CD48⁺ LSK MPP and LSK hematopoietic progenitor frequencies (Fig. 3, A to E). P0 *Tpo*^{-/-}; *Vav1-cre*; *Jak2*^{VF/Δ} mice had a significant reduction in liver CD41⁺ megakaryocytic cells and a significant increase in platelet counts compared with *Tpo*^{-/-} controls, suggesting that the JAK2 pathway mediates TPO signaling in platelet production (Fig. 3, F and G). P0 liver cells from mice with ectopically activated JAK2 also had a similar capacity to form hematopoietic colonies in vitro in methylcellulose assays (Fig. 3H). Compared with littermate *Tpo*^{-/-} controls, P0 liver cells with ectopic activation of JAK2 in *Tpo*^{-/-}; *Jak2*^{VF/+} or *Tpo*^{-/-}; *Vav1-cre*; *Jak2*^{VF/Δ} mice had a significant decrease in reconstitution capacity when transplanted into lethally irradiated recipient mice (Fig. 3I), indicating a lack of HSC rescue. Instead, a further depletion of HSC function was observed in a dose-dependent manner. Together, these data suggest that JAK2 is not a major pathway mediating the TPO signaling for HSC maintenance during development.

Ectopic activation of the MAPK pathway does not rescue HSCs in P0 *Tpo*^{-/-} mice

The MAPK pathway has also been proposed to mediate the TPO signaling (16). We tested whether the MAPK pathway mediates HSC maintenance downstream of TPO by expressing BRAF^{V600E}, which constitutively activates the MAPK pathway (24). Germline *Braf*^{V600E} expression leads to E7.5 lethality (25), and hematopoietic *Braf*^{V600E} expression driven by *Vav1-cre* causes E12.5 lethality (26), preventing a direct assessment of the role of *Braf*^{V600E} in HSCs throughout development. Using a Cre-activatable *Braf*^{V600E} (*Braf*^{CA}) allele (27), we circumvented these issues by conditionally expressing *Braf*^{V600E} through treating *Rosa26*^{creER}; *Braf*^{CA} mice with tamoxifen after E12.5. Because of delivery-related neonatal lethality associated with tamoxifen (28), we analyzed treated mice at perinatal stage E18.5. Tamoxifen administration resulted in efficient recombination of *Braf*^{CA} and expression of the *Braf*^{V600E} allele in HSCs (fig. S4M). Compared with littermate nonrecombined *Braf*^{CA} controls, conditional expression of *Braf*^{V600E} alone did not affect E18.5 liver cellularity but led to significant reductions in HSC frequency and number

(Fig. 4, A to C). It also led to significant increases in MPP and LSK hematopoietic progenitor frequencies (Fig. 4, D and E). However, the expression of *Braf*^{V600E} in *Tpo*^{-/-} mice did not lead to any significant increases in HSC frequency or number in *Tpo*^{-/-} mice (Fig. 4, B and C). CD41⁺ megakaryocytic cells were significantly increased in tamoxifen-treated E18.5 *Tpo*^{-/-}; *Rosa26*^{creER}; *Braf*^{V600E} mice, suggesting that the MAPK pathway mediates TPO signaling in megakaryocytic cell production (Fig. 4F). Liver cells from tamoxifen-treated E18.5 *Tpo*^{-/-}; *Rosa26*^{creER}; *Braf*^{V600E} formed similar numbers and types of colonies as those from *Tpo*^{-/-} littermate controls (Fig. 4G). In addition, ectopic expression of *Braf*^{V600E} did not lead to higher reconstitution capacity of HSCs from *Tpo*^{-/-} mice when transplanted into lethally irradiated recipient mice (Fig. 4H). These data suggest that the MAPK pathway is not a major mediator of the TPO signaling for HSC maintenance during development.

Ectopic activation of the mTOR pathway rescues HSCs in P0 *Tpo*^{-/-} mice

mTOR has been proposed to act downstream of the TPO signaling (16). However, it is not known whether it mediates TPO signaling in HSCs in vivo. To test this, we ectopically activated the mTOR pathway by conditionally deleting *Tsc1*, a negative regulator of the pathway, from HSCs through generating *Vav1-cre*; *Tsc1*^{fl/fl} mice. *Tsc1* was effectively recombined from HSCs (fig. S5A). Compared with wild-type littermate controls, P0 *Vav1-cre*; *Tsc1*^{fl/fl} mice had normal liver cellularity but significantly increased HSC and hematopoietic progenitor frequencies, numbers, and HSC cell size (Fig. 5, A to E, and fig. S5B). Conditional deletion of *Tsc1* led to a significant 3.5-fold increase in HSC frequency and a threefold increase in HSC number in P0 livers from *Tpo*^{-/-}; *Vav1-cre*; *Tsc1*^{fl/fl} mice relative to *Tpo*^{-/-} controls, respectively (Fig. 5, B and C, and fig. S5C). The magnitude of the increase was significantly more than that of *Vav1-cre*; *Tsc1*^{fl/fl} mice compared with wild type, suggesting a cooperative effect between *Tpo* and *Tsc1* deletion on HSCs (Fig. 5B). We observed a significant rescue of HSC cell size in *Tpo*^{-/-}; *Vav1-cre*; *Tsc1*^{fl/fl} mice to an extent similar to that of wild-type controls (Fig. 5F). *Tsc1* deletion also led to an increase in CD41⁺ cell frequency but a decrease in platelet counts in P0 *Tpo*^{-/-}; *Vav1-cre*; *Tsc1*^{fl/fl} mice compared with *Tpo*^{-/-} mice (Fig. 5, G and H). The bone marrow and spleens from *Tpo*^{-/-}; *Vav1-cre*; *Tsc1*^{fl/fl} mice had comparable HSC frequencies and numbers relative to *Tpo*^{-/-} controls (fig. S5, D to G), suggesting that the rescue of HSCs in P0 livers was not due to abnormal migration.

P0 liver cells from *Tpo*^{-/-}; *Vav1-cre*; *Tsc1*^{fl/fl} mice formed significantly more hematopoietic colonies, particularly multipotent granulocyte, erythroid, macrophage, and megakaryocyte (GEMM) colonies, compared with *Tpo*^{-/-} mice (Fig. 5I). Consistent with previous reports that deletion of *Tsc1* depletes adult HSCs (29, 30), liver cells from P0 *Vav1-cre*; *Tsc1*^{fl/fl} mice had a significant reduction in reconstituting lethally irradiated recipient mice after transplanted into an adult environment (fig. S5H). HSCs from P0 *Tpo*^{-/-}; *Vav1-cre*; *Tsc1*^{fl/fl} mice had an initial increase in reconstitution activity compared with *Tpo*^{-/-} controls (Fig. 5J). However, over time, the effect diminished, likely due to the transition of perinatal HSCs to adult identity in the environment of the adult recipient mice (Fig. 5J), since adult HSCs require *Tsc1* (fig. S5H) (29, 30). At the end of the transplantation, we confirmed high deletion efficiency by performing genotyping polymerase chain reaction (PCR) on colonies formed from single donor-type HSCs (fig. S5I).

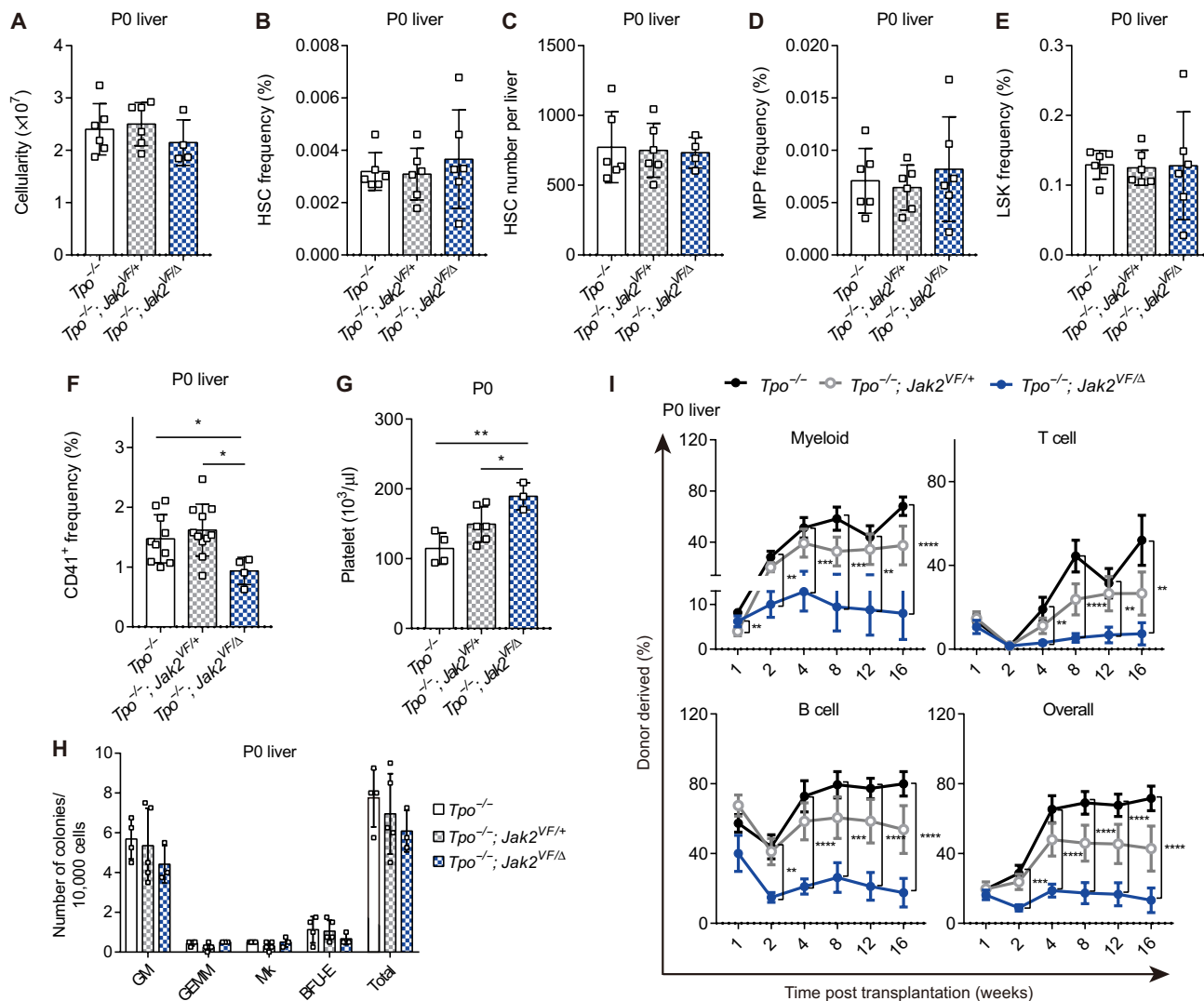


Fig. 3. Ectopic activation of the *Jak2* pathway does not rescue HSCs in *Tpo*^{-/-} mice. (A to F) Cellularity (A), CD150⁺CD48⁻LSK HSC frequency (B), number (C), CD150⁺CD48⁻LSK MPP frequency (D), LSK cell frequency (E), and CD41⁺ cell frequency (F) in P0 livers from *Tpo*^{-/-}, *Tpo*^{-/-}; *Jak2*^{VF/+}, and *Vav1-cre*; *Jak2*^{VF/CA} (*Tpo*^{-/-}; *Jak2*^{VF/ Δ) mice ($n = 5$ to 10 mice for *Tpo*^{-/-}, $n = 5$ to 11 mice for *Tpo*^{-/-}; *Jak2*^{VF/+}, and $n = 4$ to 6 mice for *Tpo*^{-/-}; *Jak2*^{VF/ Δ). (G) P0 *Tpo*^{-/-}; *Jak2*^{VF/ Δ mice had significant increase in platelet counts compared with *Tpo*^{-/-} or *Tpo*^{-/-}; *Jak2*^{VF/+} littermates ($n = 3$ to 6 mice for each condition). (H) Numbers of colonies formed by 10,000 P0 liver cells, scored as CFU-GM, CFU-GEMM, CFU-MK, or BFU-E ($n = 3$ to 6 mice for each condition). (I) A total of 5×10^5 P0 liver cells from *Tpo*^{-/-}; *Jak2*^{VF/ Δ mice gave significantly lower levels of reconstitution in irradiated mice relative to *Tpo*^{-/-} control mice (data represent means \pm SEM from two independent experiments with a total of $n = 7$ to 10 recipients for each genotype). +, wild-type allele; -, germline-deleted allele; CA, unrecombined *Jak2*^{V617F} conditional allele; VF, recombined *Jak2*^{V617F} germline allele; and Δ , *Vav1-Cre*-recombined *Jak2*^{V617F} conditional allele. *Tpo*^{-/-} includes *Vav1-cre*; *Tpo*^{-/-}, *Tpo*^{-/-}; *Jak*^{CA/+}, and *Tpo*^{-/-}. *Tpo*^{-/-}; *Jak2*^{VF/+} includes *Vav1-cre*; *Tpo*^{-/-}; *Jak2*^{VF/+} and *Tpo*^{-/-}; *Jak2*^{VF/+}. All data represent means \pm SD unless noted. Two-tailed Student's *t* tests were used to evaluate statistical significance. * $P < 0.05$; ** $P < 0.01$; *** $P < 0.001$; **** $P < 0.0001$.}}}}

To understand the underlying molecular mechanisms of HSC rescue, we performed RNA-seq analyses on sorted HSCs from P0 *Tpo*^{-/-}; *Vav1-cre*; *Tsc1*^{fl/fl} and control *Tpo*^{-/-} mice. We identified 208 down-regulated and 363 up-regulated genes in HSCs from *Tpo*^{-/-}; *Vav1-cre*; *Tsc1*^{fl/fl} mice compared with *Tpo*^{-/-} mice (fig. S6A). *Tsc1* was significantly down-regulated (fig. S6B), validating high deletion efficiency in HSCs from *Tpo*^{-/-}; *Vav1-cre*; *Tsc1*^{fl/fl} mice. Conditional deletion of *Tsc1* led to up-regulation of gene sets related to translation and amino acid metabolism associated with the mTOR pathway (fig. S6, C and D), suggesting a rescue of the metabolically active state. We found that deletion of *Tsc1* from HSCs significantly

rescued the expression of HSC signature genes caused by *Tpo* deletion in *Tpo*^{-/-}; *Vav1-cre*; *Tsc1*^{fl/fl} mice (Fig. 5K). Together, our data suggest that ectopically activating mTOR rescues HSC depletion in P0 *Tpo*^{-/-} mice in vivo. Therefore, the mTOR pathway is a major mediator of the TPO signaling for HSC maintenance during development.

TPO and LIN28B cooperate to promote mTOR activation and HSC maintenance during development

Our data suggest that TPO maintains metabolically active HSCs through promoting the mTOR pathway at P0 but not E14.5 (Fig. 2).

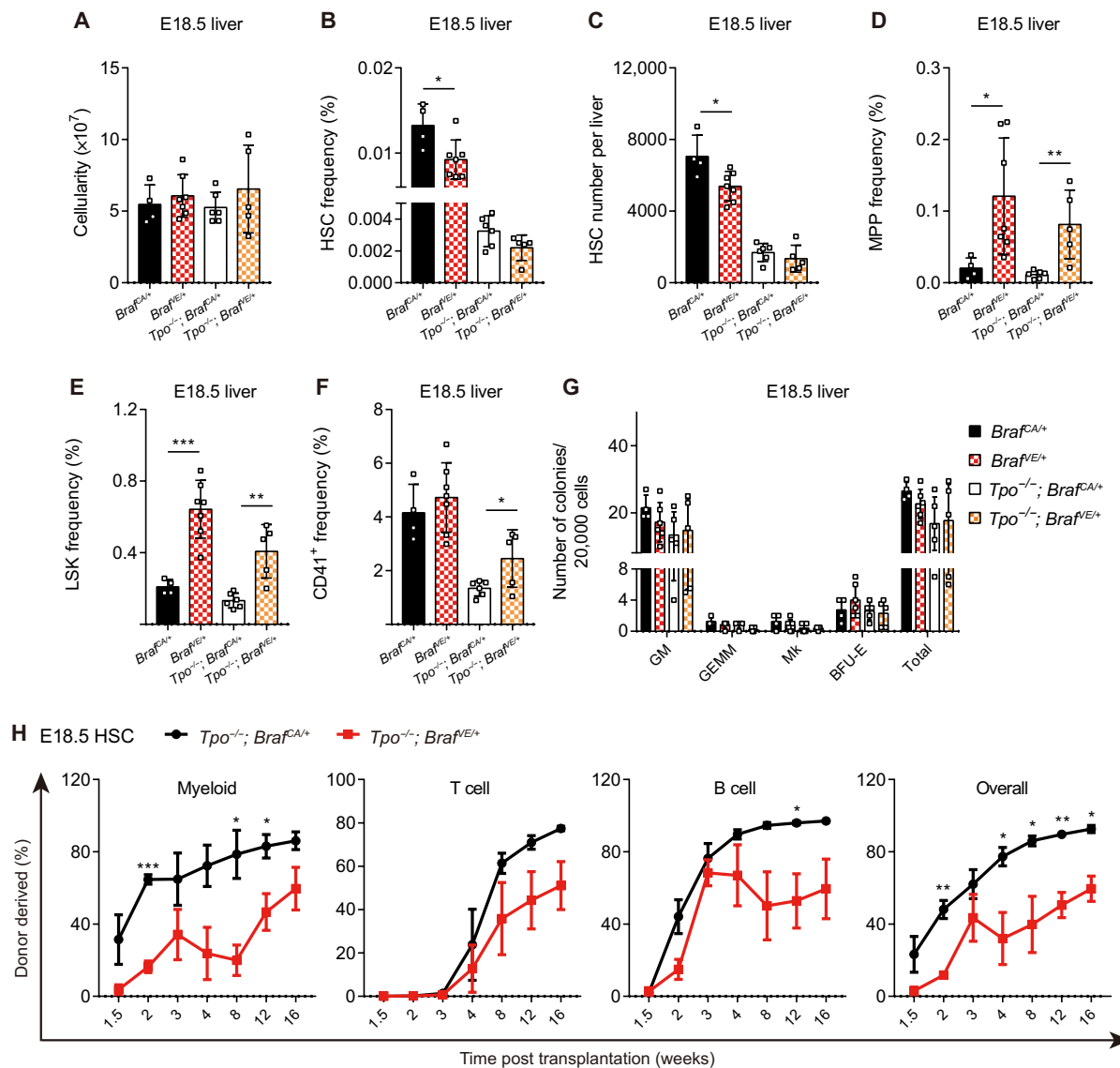


Fig. 4. Ectopic activation of BRAF does not rescue HSC number in $Tpo^{-/-}$ mice. (A to F) Cellularity (A), CD150⁺CD48⁺ LSK HSC frequency (B), number (C), CD150⁺CD48⁺ LSK MPP frequency (D), LSK cell frequency (E), and CD41⁺ cell frequency (F) in E18.5 livers from $Braf^{CA/+}$, $Braf^{VE/+}$, $Tpo^{-/-}; Braf^{CA/+}$, and $Tpo^{-/-}; Braf^{VE/+}$ embryos ($n=4$ to 7 embryos for each condition). (G) Numbers of colonies formed from 20,000 E18.5 liver cells, scored as CFU-GM, CFU-GEMM, CFU-MK, or BFU-E ($n=4$ to 6 embryos for each condition). (H) Competitive transplantation of sorted HSCs from E18.5 $Tpo^{-/-}; Braf^{CA/+}$ or $Tpo^{-/-}; Braf^{VE/+}$ embryos with the bone marrow cells. HSCs isolated from $Tpo^{-/-}; Braf^{CA/+}$ or $Tpo^{-/-}; Braf^{VE/+}$ livers were mixed with 600,000 bone marrow cells and transplanted into two lethally irradiated recipient mice per donor (data represent means \pm SEM from two independent experiments with a total of $n=3$ recipients for $Tpo^{-/-}; Braf^{CA/+}$ and $n=3$ recipients for $Tpo^{-/-}; Braf^{VE/+}$). +, wild-type allele; -, germline-deleted allele; CA, nonrecombined Cre-activatable *Braf* allele; and VE, *Braf*^{G00E} allele. All data represent means \pm SD unless noted. Two-tailed Student's *t* tests were used to evaluate statistical significance. * $P < 0.05$; ** $P < 0.01$; *** $P < 0.001$.

This raised the question of whether and how the mTOR pathway is activated at E14.5. We performed RNA-seq analyses on E14.5 and P0 HSCs and found that E14.5 HSCs expressed higher levels of mTOR target genes, indicating that the mTOR pathway is more activated at E14.5 (fig. S7A). This is consistent with a prior report showing that HSCs have higher mTOR activity at E14.5 compared with P14 (31). This activation does not depend on *Tpo* (Figs. 1 and 2), and there is residual mTOR activity in P0 HSCs without *Tpo* (Fig. 2K), suggesting that mTOR activation in perinatal liver HSCs also relies on *Tpo*-independent mechanisms.

To elucidate the *Tpo*-independent mechanisms of mTOR activation, we mined our RNA-seq data and observed significant down-regulation

of *Lin28b* and its target genes in P0 HSCs compared with E14.5 (Fig. 6A). These results were independently confirmed by quantitative PCR (qPCR) analyses (Fig. 6B). Since LIN28B is a master regulator of fetal HSC identity (11) and it promotes mTOR activation in other cell types (32, 33), we investigated whether *Lin28b* intrinsically maintains mTOR activity and HSCs during development in cooperation with extrinsic TPO in vivo. We generated *Vav1-cre; Lin28b*^{fl/fl} mice to conditionally delete *Lin28b* from HSCs. *Vav1-cre* efficiently recombined and deleted *Lin28b* from the hematopoietic system, including HSCs (fig. S7, B and C). Although *Lin28b* deletion alone has no effect on the numbers of hematopoietic progenitors, including HSCs, it led to significant reductions in P0 liver cellularity, HSC

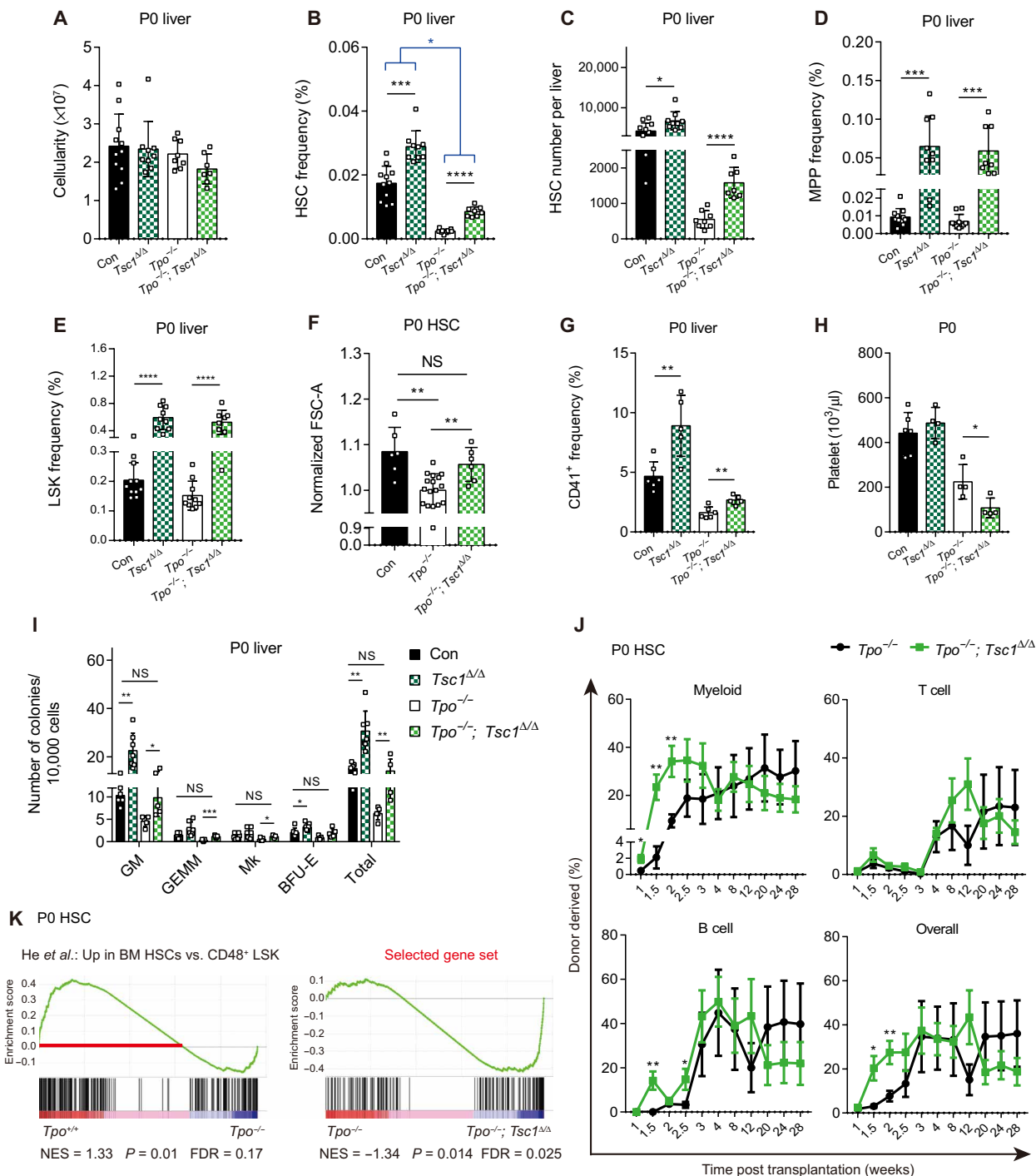


Fig. 5. Ectopic activation of the mTOR pathway rescues HSCs in *Tpo^{-/-}* mice. (A to E) Cellularity (A), CD150⁺CD48⁻LSK HSC frequency (B), number (C), CD150⁺CD48⁻LSK MPP frequency (D), and LSK cell frequency (E) in P0 livers from control, *Vav1-cre; Tsc1^{fl/fl} (Tsc1^{fl/fl})*, *Tpo^{-/-}*, and *Tpo^{-/-}; Vav1-cre; Tsc1^{fl/fl} (Tpo^{-/-}; Tsc1^{fl/fl})* mice ($n = 7$ to 11 mice for each condition). (F) Normalized FSC-A of P0 liver HSCs ($n = 6$ mice for control, $n = 17$ mice for *Tpo^{-/-}*, and $n = 6$ mice for *Tpo^{-/-}; Tsc1^{fl/fl}*). (G) CD41⁺ cell frequency in P0 livers ($n = 5$ to 6 mice for each condition). (H) Platelet counts in the peripheral blood of P0 mice ($n = 4$ to 6 mice for each condition). (I) Numbers of colonies formed from 10,000 P0 liver cells, scored as CFU-GM, CFU-GEMM, CFU-MK, or BFU-E ($n = 5$ to 7 mice for each condition). (J) Competitive transplantation of sorted HSCs from P0 *Tpo^{-/-}* or *Tpo^{-/-}; Tsc1^{fl/fl}* mice with the bone marrow cells (data represent means \pm SEM from three independent experiments with a total of $n = 6$ recipients for *Tpo^{-/-}* and $n = 6$ recipients for *Tpo^{-/-}; Tsc1^{fl/fl}*). (K) GSEA showing significant enrichment of TPO-dependent HSC signature genes (underlined in red) in *Tpo^{-/-}; Tsc1^{fl/fl}* HSCs compared with *Tpo^{-/-}* HSCs. The HSC signature genes were obtained from (46). -, germline-deleted allele; fl, *Tsc1* conditional allele; and Δ , *Vav1-Cre*-recombined *Tsc1* conditional allele. Control includes *Tsc1^{+/+}* (+, wild-type allele), *Vav1-cre; Tsc1^{+/+}*, *Tsc1^{fl/fl}*, and *Tsc1^{fl/fl}*. *Tpo^{-/-}* includes *Tpo^{-/-}*; *Tsc1^{+/+}*, *Tpo^{-/-}; Tsc1^{fl/fl}*, and *Tpo^{-/-}; Tsc1^{fl/fl}*. All data represent means \pm SD unless otherwise noted. Two-tailed Student's *t* tests or two-way analysis of variance (ANOVA) [in (B)] was used to evaluate statistical significance. * $P < 0.05$; ** $P < 0.01$; *** $P < 0.001$; **** $P < 0.0001$. NS, not significant.

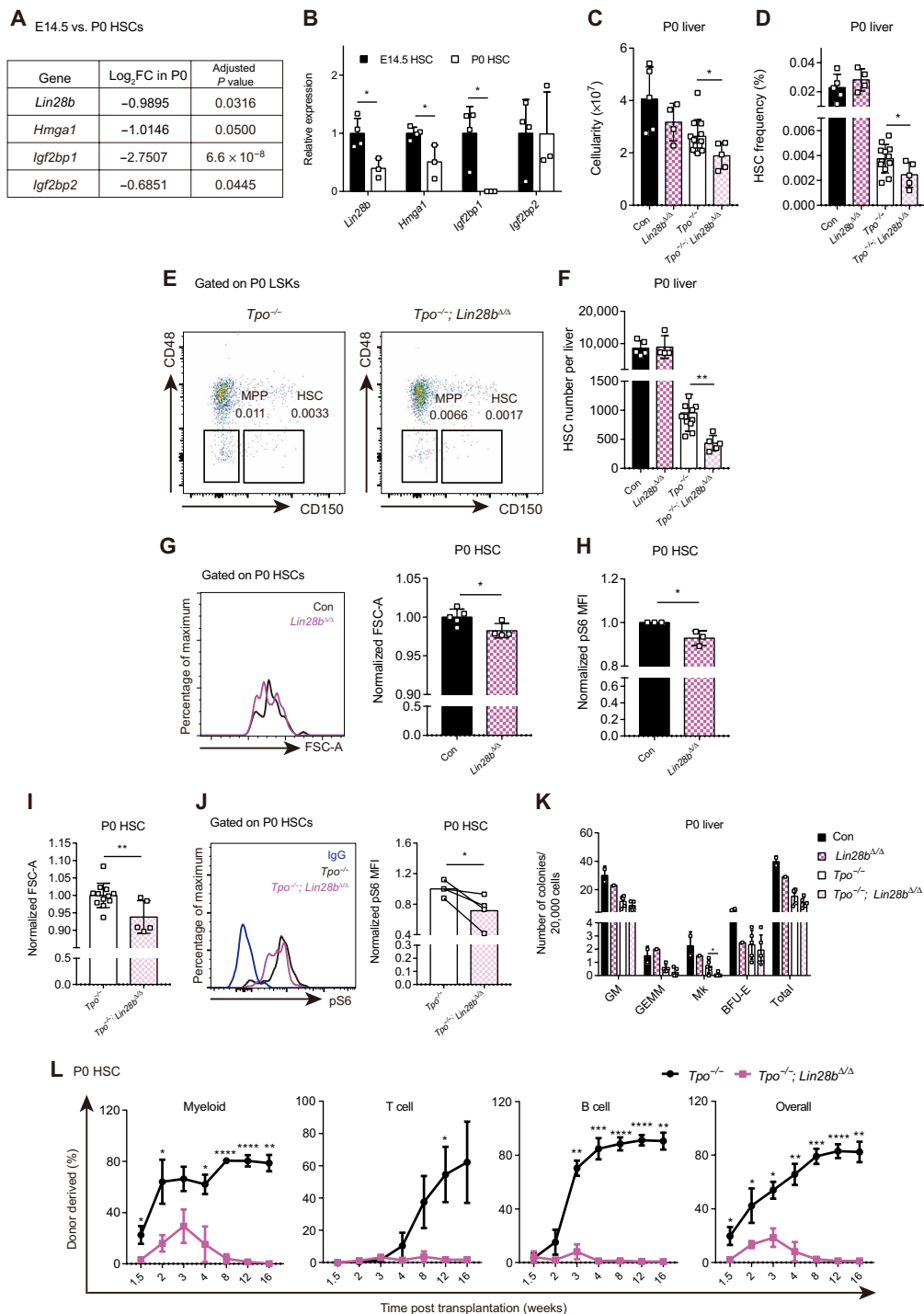


Fig. 6. TPO and LIN28B cooperatively maintain perinatal HSCs. (A) RNA-seq analysis showing expression levels of *Lin28b* and its target genes in P0 compared with E14.5 HSCs. (B) qRT-PCR analysis showing expression levels of *Lin28b* and its target genes ($n = 4$ to 5). (C and D) Cellularity (C) and HSC frequency (D) in P0 livers from control, *Vav1-cre; Lin28b^{fl/fl}* (*Lin28b^{ΔΔ}*), *Tpo^{-/-}*, and *Tpo^{-/-}; Vav1-cre; Lin28b^{fl/fl}* (*Tpo^{-/-}; Lin28b^{ΔΔ}*) mice ($n = 4$ to 12 mice for each condition). (E) Representative FACS plots showing CD150⁺CD48⁻LSK MPP and CD150⁺CD48⁺LSK HSC frequency in P0 livers. (F) HSC number in P0 livers ($n = 4$ to 12 mice for each condition). (G) Normalized FSC-A of P0 liver HSCs ($n = 4$ to 5 mice for each condition). (H) Quantification of the mean fluorescence intensity (MFI) of pS6 in P0 HSCs ($n = 3$ mice for each genotype). (I) Normalized FSC-A of P0 liver HSCs ($n = 5$ to 12 mice for each condition). (J) Quantification of the MFI of pS6 in HSCs with representative FACS plots ($n = 4$ mice for each condition). (K) Numbers of colonies formed from 20,000 P0 liver cells ($n = 4$ to 5 mice for each condition). (L) Competitive transplantation of sorted HSCs from P0 *Tpo^{-/-}* mice or *Tpo^{-/-}; Lin28b^{ΔΔ}* mice along with competitor bone marrow cells (data represent means \pm SEM from two independent experiments with a total of $n = 3$ to 4 recipients for each genotype). $-$, germline-deleted allele; *fl*, *Lin28b* conditional allele; and Δ , *Vav1-Cre*-recombined *Lin28b* conditional allele. Control includes *Lin28b^{+/+}* (+, wild-type allele), *Vav1-cre; Lin28b^{+/+}*, *Lin28b^{fl/fl}*, and *Lin28b^{fl/fl}; Tpo^{-/-}*. *Tpo^{-/-}* includes *Tpo^{-/-}; Lin28b^{+/+}*, *Tpo^{-/-}; Vav1-cre; Lin28b^{+/+}*, *Tpo^{-/-}; Lin28b^{fl/fl}*, and *Tpo^{-/-}; Lin28b^{fl/fl}*. All data represent means \pm SD unless noted. Two-tailed Student's *t* tests were used to evaluate statistical significance. * $P < 0.05$; ** $P < 0.01$; *** $P < 0.001$; **** $P < 0.0001$.

frequency, and number without affecting MPP and LSK frequencies in $Tpo^{-/-}$; $Vav1$ -cre; $Lin28b^{fl/fl}$ mice compared with $Tpo^{-/-}$ littermate controls (Fig. 6, C to F, and fig. S7, D and E). A similar cooperation between $Lin28b$ and Tpo deletion on HSCs was also observed at E14.5 (fig. S7, F to H), indicating that the Tpo signaling is active at this stage. Consistently, Mpl was expressed by E14.5 HSCs, albeit at a lower level compared with P0 (fig. S7I). There was a significant reduction in platelet counts in P0 $Tpo^{-/-}$; $Vav1$ -cre; $Lin28b^{fl/fl}$ mice compared with $Tpo^{-/-}$ littermate controls, although no significant reduction in CD41⁺ megakaryocytic cells was observed (fig. S7, J and K).

Consistent with the role of LIN28B in promoting mTOR activity, we observed modest but significant reductions in HSC cell size and pS6 levels in P0 $Vav1$ -cre; $Lin28b^{fl/fl}$ mice compared with littermate controls (Fig. 6, G and H). Compared with $Tpo^{-/-}$ mice, deletion of $Lin28b$ led to a further reduction in HSC cell size in $Tpo^{-/-}$; $Vav1$ -cre; $Lin28b^{fl/fl}$ mice (Fig. 6I). We also observed a significant reduction in pS6 staining in P0 HSCs from $Tpo^{-/-}$; $Vav1$ -cre; $Lin28b^{fl/fl}$ mice compared with $Tpo^{-/-}$ controls (Fig. 6J), suggesting that LIN28B cooperatively promotes mTOR activity with TPO. P0 liver cells from $Tpo^{-/-}$; $Vav1$ -cre; $Lin28b^{fl/fl}$ mice had an equivalent capacity to form hematopoietic colonies in vitro, except for a significant reduction in megakaryocyte colony, compared with $Tpo^{-/-}$ mice (Fig. 6K). Deletion of $Lin28b$ alone led to a modest reduction in the capacity of P0 liver cells in reconstituting lethally irradiated recipient mice (fig. S7L), suggesting that substantial HSC activity is still present without $Lin28b$. Deletion of both $Lin28b$ and Tpo resulted in a complete depletion of HSC reconstitution activity in livers from P0 $Tpo^{-/-}$; $Vav1$ -cre; $Lin28b^{fl/fl}$ mice compared with $Tpo^{-/-}$ controls (Fig. 6L). These data strongly indicate that extrinsic TPO signaling maintains appropriate mTOR activity and promote HSC maintenance during development by cooperating with intrinsic LIN28B in vivo (fig. S7M).

DISCUSSION

Although it has been reported that TPO is required by adult but not E14.5 fetal HSCs, the specific stage of the transition was not identified (13). This fetal versus adult difference has been attributed to the role of TPO in maintaining adult HSC quiescence, hinting that the transition may occur at the fetal-to-adult cell fate shift. Here, we found that during fetal development, HSCs transition to depend on extrinsic TPO around E16.5 in the liver (Fig. 1), when HSCs begin to express adult gene signatures (3). Thus, our work demonstrates that HSCs rely on distinct extrinsic factors during development and provides functional evidence of a prenatal fetal-to-adult HSC identity transition. TPO promotes adult HSC quiescence. We show that independent from regulating cell cycle, extrinsic TPO pathway gradually gains control on HSCs through regulating mTOR, metabolism, and differentiation by cooperatively functioning with intrinsic factor LIN28B during development (Figs. 2, 5, and 6). Further investigation is needed to reveal the underlying mechanisms of distinct effects of TPO on fetal versus adult HSCs. Many studies in the field used germline $Tpo^{-/-}$ mice to study the role of TPO on adult HSCs. Given that TPO has a role on fetal/neonatal HSCs, caution is needed when interpreting the data. LIN28B negatively regulates *Let-7* microRNA biogenesis, which, in turn, represses the expression of several mTOR pathway components in other cellular context (33). It remains to be shown whether LIN28B regulates the mTOR pathway through similar mechanisms in HSCs. Nonetheless,

since Tpo expression gradually increases (Fig. 1R) while $Lin28b$ diminishes (Fig. 6, A and B) over time, our work provides a mechanism of how tissue stem cells can readily gain extrinsic regulation (TPO) across ontogeny by tapping into an existing intrinsic pathway (LIN28B-mTOR) (fig. S7M).

It has been reported that E14.5 fetal liver cells from $Mpl^{-/-}$ mice have diminished reconstitution activity when transplanted into adult recipient mice (34). In contrast, consistent with our data, another report shows that E14.5 fetal liver cells from $Tpo^{-/-}$ mice have normal reconstitution activity (13). Although long-term reconstitution in adult recipients is the gold standard for assaying HSC function in vivo, it has limitation when assessing fetal HSC function, as HSCs will inevitably assume an adult identity quickly after the transplantation. Therefore, the long-term reconstitution defects of E14.5 $Mpl^{-/-}$ liver cells are likely due to an intrinsic role of Mpl on adult HSCs after transplantation. In addition, other studies have shown that the numbers of hematopoietic progenitors are significantly reduced at neonate but not E12 or E14.5 fetal livers from $Mpl^{-/-}$ mice, although HSCs were not analyzed (35, 36). While our work shows that deletion of Tpo alone at E14.5 does not affect HSC maintenance in the fetal liver, the Tpo signaling still contributes to HSC maintenance at this stage as revealed in Tpo and $Lin28b$ double knockout mice (fig. S7F). Because Tpo and Mpl expression increases during ontogeny (Fig. 1R and fig. S7I), it is likely that a combination of low expression of both Tpo and Mpl limits the Tpo signaling in HSCs at early developmental stages. Additional work is needed to address the role of TPO in hematopoiesis at earlier developmental stages.

Although several pathways have been proposed to mediate the TPO signaling, it was not clear what pathway is downstream of TPO in HSCs in vivo. We systematically investigated downstream mediators of the TPO signaling for HSC maintenance in vivo by ectopically activating several candidate pathways. Our work shows that enforced activation of mTOR leads to a rescue of HSCs in P0 $Tpo^{-/-}$ mice (Fig. 5). In contrast, enforced activation of the JAK2 or MAPK pathway does not rescue but exacerbates HSC depletion in $Tpo^{-/-}$ mice (Figs. 3 and 4), suggesting that mTOR is the major pathway mediating the TPO signaling in HSCs during development. More work is needed to explore whether similar downstream pathway preference is at play in adult HSCs. Although TPO regulates both thrombopoiesis and HSCs, the downstream mechanisms appear to be different. Ectopic activation of the JAK2 or MAPK pathway increases platelet counts in $Tpo^{-/-}$ mice, suggesting that these pathways may be downstream of TPO signaling in thrombopoiesis. These data suggest that HSCs have unique signaling mechanisms from differentiated cells, highlighting the importance of studying signaling in HSC-specific cellular context.

$Lin28b$ overexpression in adult HSCs confers fetal identity (11). Our results suggest that deletion of $Lin28b$ alone in perinatal HSCs only causes a mild phenotype (Fig. 6 and fig. S7). Genetic redundancy with $Lin28a$ may be one of the underlying mechanisms (37). Nonetheless, deletion of $Lin28b$ in $Tpo^{-/-}$ background leads to a severe depletion of P0 HSC function (Fig. 6L), suggesting that these two pathways cooperatively maintain HSCs during development in vivo. An HSC depletion phenotype is already evident in these mice at E14.5, although mice with single Tpo or $Lin28b$ deletion have normal HSC frequencies at this stage (fig. S7, F to H). These results further strengthen the notion that the cooperation between these pathways promotes HSC maintenance during development.

MATERIALS AND METHODS

Mice

Tpo^{fl}, *Tpo⁻*, *Tpo^{gfp}*, and *Tpo^{creER}* mice were described previously (15). *Tpo^{gfp}* mice were used as *Tpo⁻*. *Vav1-cre* (23), *Alb-cre* (38), *loxp-ZsGreen* (39), and *Braf^{CA}* (27) mice were obtained from the Jackson Laboratory and maintained on C57BL/6 background. *Afp-cre* (40) was purchased from Mutant Mouse Resource & Research Centers. *Rosa26^{creER}* mice (41) were generated and provided by T. Ludwig at Columbia University. *Jak2^{V617F}* mice (22) were generated by B. L. Ebert at Dana-Farber Cancer Institute, Harvard Medical School, and provided by N. Wang at Columbia University. *Tsc1^{fl}* mice (42) were a gift from X. Zhang at Columbia University. *Tsc1^{fl}* mice were backcrossed at least six times onto C57BL/6 background before analysis. *Lin28b^{fl}* mice (43) were a gift from J. Magee at Washington University School of Medicine. To induce Cre activity in *Tpo^{creER}* mice, 1 to 2 μg of tamoxifen dissolved in corn oil was administered one to two times to pregnant females. In the case of *Rosa^{creER}*, Cre activity was induced by oral gavaging 2 to 4 μg of tamoxifen at E13.5, E15.5, and E17.5 to pregnant females. All mice were housed in specific pathogen-free, Association for the Assessment and Accreditation of Laboratory Animal Care International-approved unit at Columbia University Medical Center. All protocols were approved by Columbia University Committee on the Institutional Animal Care and Use. Unless otherwise noted, data are means ± SD, and two-tailed Student's *t* tests were used to evaluate statistical significance (**P* < 0.05; ***P* < 0.01; ****P* < 0.001; *****P* < 0.0001).

Genotyping PCR primers

The following primers were used for genotyping: *Tpo^{fl}*, 5'-CATCTC-GCTGCTCTTAGCAGGG-3' and 5'-GAGCTGTTTGTGTTC-CAACTGG-3'; *Tpo⁻*, 5'-TTAGGGAGCAGGAGGGATCT-3' and 5'-CCCAGCTAACCAACCAATGCT-3'; *Tpo^{gfp}*, 5'-CGGACAC-GCTGAACTTGTGG-3', 5'-ACTTATTCTCAGGTGGTGACTC-3', and 5'-AGGGAGCCACTTCAGTTAGAC-3'; *Tpo^{creER}*, 5'-CCAC-CACCATGCCTAACTCT-3', 5'-GTTCTCCTCCACGTCTCCAG-3', and 5'-TCGCTAGCTGCTCTGATGAA-3'; *Vav1-cre*, 5'-AGATG-CCAGGACATCAGGAACCTG-3' and 5'-ATCAGCCACACCAG-ACACAGAGATC-3'; *Cre*, 5'-GCATTTCTGGGGATTGCTTA-3' and 5'-ATTCTCCCACCGTCAGTACG-3'; *loxp-ZsGreen*, 5'-GG-CATTAAGCAGCGTATCC-3' and 5'-AACCAGAAGTGGCACCT-GAC-3'; *Jak2^{fl}*, 5'-CGTGCATAGTGTCTGTGGAAGTC-3' and 5'-CGTGAGAGTCTGTAAGGCTCAA-3'; *Jak2^{VF}*, 5'-TCACAAG-CATTTGGTTTGAAT-3' and 5'-GACCAGTTGCTCCAGGGT-TA-3'; *Braf^{CA}*, 5'-TGAGTATTTTTGTGGCAACTGC-3' and 5'-CTCTGCTGGGAAAGCGGC-3'; *Tsc1^{fl}*, 5'-GTCACGACCG-TAGGAGAAGC-3' and 5'-GAATCAACCCACAGAGCAT-3'; *Tsc1⁻*, 5'-TCAGGAGGCCTCTTCTGCTA-3' and 5'-AGCCAAAG-CACTGTGTGATG-3'; *Lin28b^{fl}*, 5'-AAAGTTAGGGGGAGGG-GAAC-3' and 5'-TTCATCTGGCTCCTTTCTCG-3'; and *Lin28b⁻*, 5'-AAAGTTAGGGGGAGGGGAAC-3' and 5'-GTAAAGGGC-GCTTCCAGAAT-3'.

Long-term competitive reconstitution assay and limit dilution assay

A caesium-137 (JL Shepherd and Associates) or MultiRad 225 X-ray irradiator (Precision) was used to lethally irradiate (total 1050 rads in a split dose) adult recipient mice. After anesthetization, mice were retro-orbitally injected with either 5×10^5 developing liver cells and 5×10^5 recipient bone marrow cells or purified HSCs and

3×10^5 recipient bone marrow cells as noted. Mice were maintained on antibiotic water (Baytril 0.17 g liter⁻¹) for 14 days after transplantation and then changed to regular water. Recipient mice were bled periodically to evaluate the level of donor-derived hematopoietic lineages including myeloid, B, and T cells. For limit dilution assays, three doses of donor liver cells (8×10^4 , 4×10^4 , and 1.5×10^4) along with 3×10^5 recipient bone marrow cells were transplanted into lethally irradiated mice ($n = 10$ mice for *Tpo^{+/+}* 8×10^4 dose, $n = 7$ mice for *Tpo^{+/+}* 4×10^4 dose, $n = 10$ mice for *Tpo^{+/+}* 1.5×10^4 dose, $n = 10$ mice for *Tpo^{-/-}* 8×10^4 dose, $n = 9$ mice for *Tpo^{-/-}* 4×10^4 dose, and $n = 11$ mice for *Tpo^{-/-}* 1.5×10^4 dose). After 16 weeks, the percentage of mice that were not multilineage reconstituted (<0.5%) by donor hematopoietic cells was plotted against cell dose. ELDA software was used to calculate functional HSC frequency and to assess statistical significance. Blood was incubated with ammonium chloride potassium red cell lysis before proceeding to antibody staining. Cells were stained with anti-CD45.2 (104), anti-CD45.1 (A20), anti-Gr1 (8C5), anti-Mac-1 (M1/70), anti-B220 (6B2), and anti-CD3 (KT31.1) (BioLegend) and analyzed by flow cytometry.

Colony-forming unit assay

A total of 15,000 to 40,000 liver cells were plated in 1.5 ml of methylcellulose culture medium (3434, STEMCELL Technologies) and incubated at 37°C in 5% CO₂ and constant humidity. Colonies were counted 10 to 12 days after plating on an Olympus CKX41 microscope (Olympus Life Science) and scored as derived from granulocyte-macrophage progenitor cells [colony-forming unit (CFU)-GM], multipotent GEMM progenitor cells (CFU-GEMM), erythroid progenitor cells (BFU-E), and megakaryocyte progenitor cells (CFU-MK).

Flow cytometry

Liver cells were isolated by crushing the tissue between two glass slides. The cells were passed through 25-gauge syringes with Ca²⁺- and Mg²⁺-free Hanks' balanced salt solution with 2% heat-inactivated bovine serum for single-cell suspension. Then, cells were filtered through 70-μm nylon mesh. For staining HSCs, the following antibodies were used: lineage markers [anti-Ter119, anti-B220 (6B2), anti-Gr1 (8C5), anti-CD2 (RM2-5), anti-CD3 (17A2), anti-CD5 (53-7.3), and anti-CD8 (53-6.7)], anti-CD150 (TC15-12F12.2), anti-CD48 (HM48-1), anti-Sca-1 (E13-161.7), and anti-cKit (2B8) (BioLegend). For staining Flt3⁺ LSKs, the following antibodies were used: lineage markers [anti-Ter119, anti-B220 (6B2), anti-Gr1 (8C5), anti-CD2 (RM2-5), anti-CD3 (17A2), anti-CD5 (53-7.3), and anti-CD8 (53-6.7)], anti-Sca-1 (E13-161.7), anti-cKit (2B8), and anti-Flt3 (A2F10) (BioLegend). Anti-CD41 (MWReg30) (BioLegend) antibody was used to assess frequency of CD41⁺ cells. DAPI (4',6-diamidino-2-phenylindole) was used to preclude dead cells. Samples were run on BD FACSAria II, BD LSR II, BD FACSCelesta, or BD FACSCanto flow cytometers. BD FACSDiva or FlowJo (Tree Star) software was used for data analysis.

Immunostaining of liver or embryo sections

Freshly dissected livers were fixed in 4% paraformaldehyde (PFA) for 1 to 3 hours followed by overnight incubation in 30% sucrose in phosphate-buffered saline (PBS). Embryos were dissected in cold PBS, after which the skin and limbs were removed. The embryos were fixed in 4% PFA overnight at 4°C. Following fixation, the embryos were washed three times in PBS. After wash, the embryos

were decalcified in 10% EDTA solution (pH 7.3) overnight at 4°C. The following day, the embryos were moved to 30% sucrose in PBS and incubated overnight. The tissues and embryos were embedded in OCT (optimal cutting temperature) compound and snap frozen on dry ice. Liver and embryo sections were cut at 10 µm using a CryoJane system (Instrumedics) and air dried overnight at room temperature. Sections were rehydrated in PBS for 5 min and blocked using either 5% goat serum or 5% donkey serum in PBS for 30 min. Primary antibodies were applied overnight at 4°C, and then slides were incubated in secondary antibodies at room temperature for 2 hours with washes in between. Primary antibodies were rabbit anti-Laminin antibody (L9393, Sigma-Aldrich), rabbit anti-Desmin antibody (GTX103557, GeneTex), and goat anti-HNF4 α antibody (sc-6556, Santa Cruz Biotechnology). Secondary antibodies were anti-rabbit Alexa Fluor 555 (Thermo Fisher Scientific) and anti-goat Alexa Fluor 555 (Thermo Fisher Scientific). DAPI was used to stain the nuclei. Slides were mounted with ProLong Gold Antifade (Invitrogen), and images were acquired on a Nikon Ti Eclipse confocal, Leica SP8, or Zeiss Axio Observe microscope.

Quantitative PCR

Cells were sorted directly into TRIzol. Total RNA was purified according to manufacturer's instructions and subjected to reverse transcription using SuperScript III Reverse Transcriptase (Invitrogen). The levels of gene transcripts were quantified by quantitative real-time PCR using GoTaq qPCR Master Mix (Promega) on a CFX Connect Real-Time PCR Detection System (Bio-Rad). β -Actin or *Gapdh* was used to normalize the expression of genes. Primers used in this study were the following: β -actin, 5'-GCTCTTTCCAG-CCTTCCTT-3' and 5'-CTTCTGCATCCTGTCAGCAA-3'; *Gapdh*, 5'-AACTTTGGCATTGTGGAAGG-3' and 5'-ATGCAGGGAT-GATGTTCTGG-3'; *p57*, 5'-GGAGCAGGACGAGAATCAAG-3' and 5'-GAAGAAGTCGTTCCGATTTGG-3'; *p19*, 5'-GGAGCTG-GTGCATCCTGACGC-3' and 5'-TGGCACCTTGCTTCAGGAGCTC-3'; *Lin28b*, 5'-GAGTCCAGGATGATTCCAAGA-3' and 5'-TGCTCT-GACAGTAATGGCACTT-3' or 5'-TGGTTCAACGTGCGCATG-GGA-3' and 5'-CCACTGGCTCTCCTTCTTTCAAGCT-3'; *Hmgal*, 5'-GCTGGTCCGGGAGTCAGAAAG-3' and 5'-GGTGACTTTC-CGGTCTTTGG-3'; *Igf2bp1*, 5'-GGCTCAGTACGGTACAGTG-GA-3' and 5'-ACCACAGCTGTCTCACTTTTCAAG-3'; *Igf2bp2*, 5'-GGGAAAATCATGGAAGTTGACTA-3' and 5'-CGGGATGTT-CGAATCTG-3'; *Tpo*, 5'-CCTTTGTCTATCCCTGTTCTGC-3' and 5'-ACTGCCCCCTAGAATGTCCTGT-3'; and *Mpl*, 5'-CTGC-CACTTCAAGTCACGAA-3' and 5'-CACTTGAGACCTCCCTCCAG-3'.

Cell cycle and cell death analysis

For 5-bromo-2'-deoxyuridine (BrdU) incorporation analysis, P0 mice were intraperitoneally injected with 0.1 mg of BrdU per gram of body weight. The mice were euthanized 4 hours later for the analysis. The frequency of BrdU⁺ cells was determined by flow cytometry using an APC BrdU Flow Kit (BD Biosciences). For Ki67 staining, cells were fixed and permeabilized (BD Biosciences) and stained with anti-Ki67 (eBioscience, SolA15) and DAPI (1 µg/ml). Annexin V staining was performed using Annexin V Apoptosis Detection Kit APC (BioLegend, 640920) per the manufacturer's instructions.

Intracellular staining

For intracellular staining, cells were fixed in BD Cytofix/Cytoperm buffer (BD Biosciences) for 30 min on ice, washed in Perm/Wash

buffer (BD Biosciences), and permeabilized with BD CytoPerm Plus buffer (BD Biosciences) for 10 min on ice. Cells were refixed in BD Cytofix/Cytoperm buffer for 10 min on ice and washed in Perm/Wash buffer. Cells were then incubated in Perm/Wash buffer with the following primary antibodies: rabbit anti-phospho-S6 PE (Cell Signaling Technology, 5316), rabbit anti-phospho-STAT5 PE (Cell Signaling Technology, 5387), rabbit immunoglobulin G XP Isotype Control PE (Cell Signaling Technology, 5742), and anti- γ H2AX (clone 2F3; BioLegend, 613405). After staining, cells were washed in Perm/Wash buffer and resuspended in Perm/Wash buffer, followed by flow cytometry analysis.

Complete blood counts

Peripheral blood was collected by decapitation or cardiac puncture into EDTA-coated capillary tubes. Blood samples were analyzed by Genesis (Oxford Science Inc.).

Mitochondrial quantification

For mitochondrial DNA quantification, 100 to 200 HSCs were sorted into 50 µl of lysis buffer (Viagen Biotech, 102-T) with freshly added proteinase K (Fisher BioReagents, BP1700-100). Cells were incubated for 2 hours at 56°C and 15 min at 95°C. Quantification was performed by qPCR using GoTaq qPCR Master Mix (Promega) on a CFX Connect Real-Time PCR Detection System (Bio-Rad). Five microliters of cell lysate was used in each reaction. Relative mitochondrial DNA:nuclear DNA ratio was calculated using the $\Delta\Delta$ Ct method upon targeting of nuclear-encoded gene (β -actin: 5'-CGGCTTGC-GGGTGTAAAAG-3' and 5'-CGTGATCGTAGCGTCTGGTT-3') and mitochondrial-encoded gene (*Cytb*: 5'-CTTCATGTCGGAC-GAGGCTTA-3' and 5'-TGTGGCTATGACTGCGAACA-3'). For experiments with MitoTracker Green (MTG) or tetramethylrhodamine ethyl ester (TMRE), cells were incubated with MTG (100 nM; Thermo Fisher) or TMRE (20 nM; Thermo Fisher) in the presence of verapamil (50 µM; Sigma-Aldrich) at 37°C for 20 to 30 min.

Measuring protein synthesis

For in vitro analysis, cells were cultured in 100 µl of Dulbecco's modified Eagle's medium supplemented with 15% heat-inactivated fetal bovine serum, stem cell factor (100 ng/ml), interleukin-13 (IL-3; 10 ng/ml), IL-6 (10 ng/ml), 50 µM β -mercaptoethanol, and O-propargyl-puromycin (OP-Puro, 20 µM; Thermo Fisher Scientific) for 1 hour at 37°C in 5% CO₂ and constant humidity. After incubation, cells were washed with PBS and fixed in 0.5 ml of 1% PFA for 15 min on ice. Cells were washed with PBS, followed by permeabilization with 200 µl of PBS supplemented with 3% fetal bovine serum and 0.1% saponin for 5 min at room temperature. OP-Puro was detected using Click-iT Plus OPP Alexa Fluor 488 Protein Synthesis Assay Kit (Thermo Fisher Scientific, C10456) according to the manufacturer's instructions.

Western blots

A total of 20,000 to 30,000 LSK cells were sorted into trichloroacetic acid (TCA), and the volume was adjusted to a final concentration of 10% TCA. Samples were incubated for 15 min on ice and centrifuged at 14,000 revolutions per minute at 4°C for 20 min. Supernatant was carefully removed, and precipitates were washed in prechilled acetone twice. The pellets were air dried, solubilized in NuPAGE LDS Sample Buffer, and heated at 70°C for 10 min. Samples subjected to immunoblot analysis with the indicated antibodies: rabbit

anti-phospho-S6 (Cell Signaling Technology, 2215S), rabbit anti-phospho-4E-BP1 (Cell Signaling Technology, 2855S), and mouse anti- β -Actin (Thermo Fisher Scientific, MA5-15739). The immunoreactive bands were detected using horseradish peroxidase-conjugated secondary antibodies (Jackson ImmunoResearch) and enhanced chemiluminescence reagents (Thermo Fisher Scientific). Before reprobing, blots were stripped with stripping buffer [1% SDS and 25 mM glycine (pH 2)].

Gene expression profiling and analysis

For RNA-seq, libraries were prepared according to the Smart-seq2 protocol as described (44) from 100 to 200 sorted HSCs. Samples were sequenced by NextSeq 500 (Illumina) with single-end 75-base pair read length using the NextSeq 500/550 High Output v2 Kit (75 cycles; Illumina). The RNA-seq pipeline from Basepair (www.basepairtech.com) was used for the analysis. Expression count was analyzed by STAR, and differential expression by DESeq2 ($P < 0.05$ and fold change > 2). GSEA analysis was conducted as previously described (45). Transcriptomic signatures are provided in table S1.

SUPPLEMENTARY MATERIALS

Supplementary material for this article is available at <https://science.org/doi/10.1126/sciadv.abm7688>

[View/request a protocol for this paper from Bio-protocol.](#)

REFERENCES AND NOTES

1. Y. Lee, M. Decker, H. Lee, L. Ding, Extrinsic regulation of hematopoietic stem cells in development, homeostasis and diseases. *Wiley Interdiscip. Rev. Dev. Biol.* **6**, e279 (2017).
2. M. R. Copley, C. J. Eaves, Developmental changes in hematopoietic stem cell properties. *Exp. Mol. Med.* **45**, e55 (2013).
3. Y. Li, W. Kong, W. Yang, R. M. Patel, E. B. Casey, T. Okeyo-Owuor, J. M. White, S. N. Porter, S. A. Morris, J. A. Magee, Single-cell analysis of neonatal HSC ontogeny reveals gradual and uncoordinated transcriptional reprogramming that begins before birth. *Cell Stem Cell* **27**, 732–747.e7 (2020).
4. M. B. Bowie, D. G. Kent, B. Dykstra, K. D. McKnight, L. McCaffrey, P. A. Hoodless, C. J. Eaves, Identification of a new intrinsically timed developmental checkpoint that reprograms key hematopoietic stem cell properties. *Proc. Natl. Acad. Sci. U.S.A.* **104**, 5878–5882 (2007).
5. I. K. Park, D. Qian, M. Kiel, M. W. Becker, M. Pihalja, I. L. Weissman, S. J. Morrison, M. F. Clarke, Bmi-1 is required for maintenance of adult self-renewing haematopoietic stem cells. *Nature* **423**, 302–305 (2003).
6. H. Hock, M. J. Hamblen, H. M. Rooke, J. W. Schindler, S. Saleque, Y. Fujiwara, S. H. Orkin, Gfi-1 restricts proliferation and preserves functional integrity of haematopoietic stem cells. *Nature* **431**, 1002–1007 (2004).
7. H. Hock, E. Meade, S. Medeiros, J. W. Schindler, P. J. M. Valk, Y. Fujiwara, S. H. Orkin, Tel/Etv6 is an essential and selective regulator of adult hematopoietic stem cell survival. *Genes Dev.* **18**, 2336–2341 (2004).
8. H. Xie, J. Xu, J. H. Hsu, M. Nguyen, Y. Fujiwara, C. Peng, S. H. Orkin, Polycomb repressive complex 2 regulates normal hematopoietic stem cell function in a developmental-stage-specific manner. *Cell Stem Cell* **14**, 68–80 (2014).
9. M. Jones, J. Chase, M. Brinkmeier, J. Xu, D. N. Weinberg, J. Schira, A. Friedman, S. Malek, J. Grembecka, T. Cierpicki, Y. Dou, S. A. Camper, I. Maillard, Ash1 controls quiescence and self-renewal potential in hematopoietic stem cells. *J. Clin. Invest.* **125**, 2007–2020 (2015).
10. I. Kim, T. L. Saunders, S. J. Morrison, Sox17 dependence distinguishes the transcriptional regulation of fetal from adult hematopoietic stem cells. *Cell* **130**, 470–483 (2007).
11. M. R. Copley, S. Babovic, C. Benz, D. J. H. F. Knapp, P. A. Beer, D. G. Kent, S. Wohrer, D. Q. Treloar, C. Day, K. Rowe, H. Mader, F. Kuchenbauer, R. K. Humphries, C. J. Eaves, The Lin28b-let-7-Hmga2 axis determines the higher self-renewal potential of fetal haematopoietic stem cells. *Nat. Cell Biol.* **15**, 916–925 (2013).
12. J. Yuan, C. K. Nguyen, X. Liu, C. Kanellopoulou, S. A. Muljo, Lin28b reprograms adult bone marrow hematopoietic progenitors to mediate fetal-like lymphopoiesis. *Science* **335**, 1195–1200 (2012).
13. H. Qian, N. Buza-Vidas, C. D. Hyland, C. T. Jensen, J. Antonchuk, R. Månsson, L. A. Thoren, M. Eklom, W. S. Alexander, S. E. W. Jacobsen, Critical role of thrombopoietin in maintaining adult quiescent hematopoietic stem cells. *Cell Stem Cell* **1**, 671–684 (2007).
14. H. Yoshihara, F. Arai, K. Hosokawa, T. Hagiwara, K. Takubo, Y. Nakamura, Y. Gomei, H. Iwasaki, S. Matsuoka, K. Miyamoto, H. Miyazaki, T. Takahashi, T. Suda, Thrombopoietin/MPL signaling regulates hematopoietic stem cell quiescence and interaction with the osteoblastic niche. *Cell Stem Cell* **1**, 685–697 (2007).
15. M. Decker, J. Leslie, Q. Liu, L. Ding, Hepatic thrombopoietin is required for bone marrow hematopoietic stem cell maintenance. *Science* **360**, 106–110 (2018).
16. M. Abe, K. Suzuki, O. Inagaki, S. Sassa, H. Shikama, A novel MPL point mutation resulting in thrombopoietin-independent activation. *Leukemia* **16**, 1500–1506 (2002).
17. Y. Lee, J. Leslie, Y. Yang, L. Ding, Hepatic stellate and endothelial cells maintain hematopoietic stem cells in the developing liver. *J. Exp. Med.* **218**, e20200882 (2021).
18. B. de Laval, P. Pawlikowska, L. Petit-Cocault, C. Bilhou-Nabera, G. Aubin-Houzelstein, M. Souyri, F. Pouzoulet, M. Gaudry, F. Porteu, Thrombopoietin-increased DNA-PK-dependent DNA repair limits hematopoietic stem and progenitor cell mutagenesis in response to DNA damage. *Cell Stem Cell* **12**, 37–48 (2013).
19. R. A. Saxton, D. M. Sabatini, mTOR signaling in growth, metabolism, and disease. *Cell* **168**, 960–976 (2017).
20. A. Tefferi, Myeloproliferative neoplasms: A decade of discoveries and treatment advances. *Am. J. Hematol.* **91**, 50–58 (2016).
21. M. Decker, L. Martinez-Morentin, G. Wang, Y. Lee, Q. Liu, J. Leslie, L. Ding, Leptin-receptor-expressing bone marrow stromal cells are myofibroblasts in primary myelofibrosis. *Nat. Cell Biol.* **19**, 677–688 (2017).
22. A. Mullally, S. W. Lane, B. Ball, C. Megerdichian, R. Okabe, F. al-Shahrour, M. Paktinat, J. E. Haydu, E. Housman, A. M. Lord, G. Wernig, M. G. Kharas, T. Mercher, J. L. Kutok, D. G. Gilliland, B. L. Ebert, Physiological Jak2V617F expression causes a lethal myeloproliferative neoplasm with differential effects on hematopoietic stem and progenitor cells. *Cancer Cell* **17**, 584–596 (2010).
23. J. de Boer, A. Williams, G. Skavdis, N. Harker, M. Coles, M. Tolaini, T. Norton, K. Williams, K. Roderick, A. J. Potocnik, D. Kioussis, Transgenic mice with hematopoietic and lymphoid specific expression of Cre. *Eur. J. Immunol.* **33**, 314–325 (2003).
24. M. J. Garnett, R. Marais, Guilty as charged. *Cancer Cell* **6**, 313–319 (2004).
25. K. Mercer, S. Giblett, S. Green, D. Lloyd, S. DaRocha Dias, M. Plumb, R. Marais, C. Pritchard, Expression of endogenous oncogenic V600E-raf induces proliferation and developmental defects in mice and transformation of primary fibroblasts. *Cancer Res.* **65**, 11493–11500 (2005).
26. S. S. Chung, E. Kim, J. H. Park, Y. R. Chung, P. Lito, J. Teruya-Feldstein, W. Hu, W. Beguelin, S. Monette, C. Duy, R. Rampal, L. Telis, M. Patel, M. K. Kim, K. Huberman, N. Bouvier, M. F. Berger, A. M. Melnick, N. Rosen, M. S. Tallman, C. Y. Park, O. Abdel-Wahab, Hematopoietic stem cell origin of BRAFV600E mutations in hairy cell leukemia. *Sci. Transl. Med.* **6**, 238ra271 (2014).
27. D. Dankort, E. Filenova, M. Collado, M. Serrano, K. Jones, M. McMahon, A new mouse model to explore the initiation, progression, and therapy of BRAFV600E-induced lung tumors. *Genes Dev.* **21**, 379–384 (2007).
28. P. S. Danielian, D. Muccino, D. H. Rowitch, S. K. Michael, A. P. McMahon, Modification of gene activity in mouse embryos in utero by a tamoxifen-inducible form of Cre recombinase. *Curr. Biol.* **8**, 1323–1352 (1998).
29. B. Gan, E. Sahin, S. Jiang, A. Sanchez-Aguilera, K. L. Scott, L. Chin, D. A. Williams, D. J. Kwiatkowski, R. A. DePinho, mTORC1-dependent and -independent regulation of stem cell renewal, differentiation, and mobilization. *Proc. Natl. Acad. Sci. U.S.A.* **105**, 19384–19389 (2008).
30. C. Chen, Y. Liu, R. Liu, T. Ikenoue, K. L. Guan, Y. Liu, P. Zheng, TSC-mTOR maintains quiescence and function of hematopoietic stem cells by repressing mitochondrial biogenesis and reactive oxygen species. *J. Exp. Med.* **205**, 2397–2408 (2008).
31. J. A. Magee, T. Ikenoue, D. Nakada, J. Y. Lee, K. L. Guan, S. J. Morrison, Temporal changes in PTEN and mTORC2 regulation of hematopoietic stem cell self-renewal and leukemia suppression. *Cell Stem Cell* **11**, 415–428 (2012).
32. X. J. Li, A. Doetzlhofer, Lin28b/let-7 control the ability of neonatal murine auditory supporting cells to generate hair cells through mTOR signaling. *Proc. Natl. Acad. Sci. U.S.A.* **117**, 22225–22236 (2020).
33. H. Zhu, N. Shyh-Chang, A. V. Segrè, G. Shinoda, S. P. Shah, W. S. Einhorn, A. Takeuchi, J. M. Engreitz, J. P. Hagan, M. G. Kharas, A. Urbach, J. E. Thornton, R. Triboulet, R. I. Gregory, DIAGRAM Consortium, MAGIC Investigators, D. Altshuler, G. Q. Daley, The Lin28/let-7 axis regulates glucose metabolism. *Cell* **147**, 81–94 (2011).
34. L. Petit-Cocault, C. Volle-Challier, M. Fleury, B. Peault, M. Souyri, Dual role of Mpl receptor during the establishment of definitive hematopoiesis. *Development* **134**, 3031–3040 (2007).
35. W. S. Alexander, A. W. Roberts, N. A. Nicola, R. Li, D. Metcalf, Deficiencies in progenitor cells of multiple hematopoietic lineages and defective megakaryocytopoiesis in mice lacking the thrombopoietin receptor c-Mpl. *Blood* **87**, 2162–2170 (1996).
36. J. Antonchuk, C. D. Hyland, D. J. Hilton, W. S. Alexander, Synergistic effects on erythropoiesis, thrombopoiesis, and stem cell competitiveness in mice deficient in thrombopoietin and steel factor receptors. *Blood* **104**, 1306–1313 (2004).
37. N. Shyh-Chang, G. Q. Daley, Lin28: Primal regulator of growth and metabolism in stem cells. *Cell Stem Cell* **12**, 395–406 (2013).

38. C. M. Weisend, J. A. Kundert, E. S. Suvorova, J. R. Prigge, E. E. Schmidt, Cre activity in fetal albCre mouse hepatocytes: Utility for developmental studies. *Genesis* **47**, 789–792 (2009).
39. L. Madisen, T. A. Zwingman, S. M. Sunkin, S. W. Oh, H. A. Zariwala, H. Gu, L. L. Ng, R. D. Palmiter, M. J. Hawrylycz, A. R. Jones, E. S. Lein, H. Zeng, A robust and high-throughput Cre reporting and characterization system for the whole mouse brain. *Nat. Neurosci.* **13**, 133–140 (2010).
40. L. Zhang, N. E. Rubins, R. S. Ahima, L. E. Greenbaum, K. H. Kaestner, Foxa2 integrates the transcriptional response of the hepatocyte to fasting. *Cell Metab.* **2**, 141–148 (2005).
41. C. de Luca, T. J. Kowalski, Y. Zhang, J. K. Elmquist, C. Lee, M. W. Kilimann, T. Ludwig, S. M. Liu, S. C. Chua Jr., Complete rescue of obesity, diabetes, and infertility in db/db mice by neuron-specific LEPR-B transgenes. *J. Clin. Invest.* **115**, 3484–3493 (2005).
42. D. J. Kwiatkowski, H. Zhang, J. L. Bandura, K. M. Heiberger, M. Glogauer, N. el-Hashemite, H. Onda, A mouse model of TSC1 reveals sex-dependent lethality from liver hemangiomas, and up-regulation of p70S6 kinase activity in Tsc1 null cells. *Hum. Mol. Genet.* **11**, 525–534 (2002).
43. G. Shinoda, N. Shyh-Chang, T. Y. de Soysa, H. Zhu, M. T. Seligson, S. P. Shah, N. Abo-Sido, A. Yabuuchi, J. P. Hagan, R. I. Gregory, J. M. Asara, L. C. Cantley, E. G. Moss, G. Q. Daley, Fetal deficiency of lin28 programs life-long aberrations in growth and glucose metabolism. *Stem Cells* **31**, 1563–1573 (2013).
44. S. Picelli, O. R. Faridani, Å. K. Björklund, G. Winberg, S. Sagasser, R. Sandberg, Full-length RNA-seq from single cells using Smart-seq2. *Nat. Protoc.* **9**, 171–181 (2014).
45. A. Subramanian, P. Tamayo, V. K. Mootha, S. Mukherjee, B. L. Ebert, M. A. Gillette, A. Paulovich, S. L. Pomeroy, T. R. Golub, E. S. Lander, J. P. Mesirov, Gene set enrichment analysis: A knowledge-based approach for interpreting genome-wide expression profiles. *Proc. Natl. Acad. Sci. U.S.A.* **102**, 15545–15550 (2005).
46. S. He, I. Kim, M. S. Lim, S. J. Morrison, Sox17 expression confers self-renewal potential and fetal stem cell characteristics upon adult hematopoietic progenitors. *Genes Dev.* **25**, 1613–1627 (2011).

Acknowledgments: We thank X. Zhang at Columbia University for sharing *Tsc1^{fl}* mice, B. Ebert at Harvard University and N. Wang at Columbia University for sharing *Jak2^{V167F}* mice, and J. Magee at Washington University for sharing *Lin28b^{fl}* mice. We thank A. Figueroa at the Department of Microbiology and Immunology and M. Kissner at the Columbia Stem Cell Initiative for flow cytometry as well as T. Swayne and L. Munteanu at the Columbia University Confocal and Specialized Microscopy core for confocal microscopy. **Funding:** This work was supported by the Rita Allen Foundation, the Schaefer Scholars program, and the National Heart, Lung, and Blood Institute (R01HL132074 and R01HL153487). L.D. was supported by a Scholar Award from the Leukemia & Lymphoma Society and R01HL155868. Y.L. was supported by the Korea Foundation for Advanced Studies and the NYSTEM Columbia training program in stem cell research. This research was funded in part through the NIH/NCI Cancer Center Support Grant P30CA013696. **Author contributions:** Y.L. and L.D. performed all of the experiments with help from E.D.-M. and J.L. Y.L. and L.D. designed the experiments, interpreted the results, and wrote the manuscript. **Competing interests:** The authors declare that they have no competing interests. **Data and materials availability:** All data needed to evaluate the conclusions in the paper are present in the paper and/or the Supplementary Materials. RNA-seq data have been deposited to the Gene Expression Omnibus under accession number GSE172393.

Submitted 10 October 2021

Accepted 25 January 2022

Published 16 March 2022

10.1126/sciadv.abm7688